Solid-State Electronics 109 (2015) 12–16

Contents lists available at ScienceDirect

Solid-State Electronics

journal homepage: www.elsevier.com/locate/sse

Analysis of different forward current–voltage behaviours of Al implanted 4H-SiC vertical p–i–n diodes

M.L. Megherbi [a], F. Pezzimenti [b], L. Dehimi [a,c], S. Rao [b,*], F.G. Della Corte [b]

[a] Laboratory of Metallic and Semiconducting Materials, Mohammed Kheider University, 07000 Biskra, Algeria
[b] DIIES – Università Mediterranea di Reggio Calabria, Via Graziella, 89122 Reggio Calabria, Italy
[c] Faculty of Science, Elhadj Lakhdar University, 05000 Batna, Algeria

ARTICLE INFO

Article history:
Received 27 September 2014
Received in revised form 18 February 2015
Accepted 2 March 2015

Keywords:
p–i–n diode
Silicon carbide
Device simulation
Carrier lifetime

ABSTRACT

In this work different experimental current–voltage behaviours of several Al implanted 4H-SiC p–i–n diodes are investigated by means of numerical simulations in a wide range of currents and temperatures. Some devices for which recombination and tunneling are the dominant current processes at all biases are classified as "leaky" diodes. The well behaved diodes, instead, show good rectifying characteristics with a current conduction due to tunneling below 1.7 V, recombination between 1.7 V and 2.5 V, and diffusion processes above 2.5 V. At higher current regimes, a series resistance in excess of 1 $m\Omega\,cm^2$ becomes the main current limiting factor. Depending on the relative weight between the contact resistances and the internal diode resistance, different temperature dependencies of the current are obtained. A good agreement between numerical and measured data is achieved employing temperature-dependent carrier lifetime and mobility as fitting parameters.

1. Introduction

Silicon carbide (SiC) is a wide band-gap semiconductor with interesting physical properties in order to realize electronic devices well suited to operate under high-temperature, high-power, and/or high-radiation conditions. The potentials of the 4H-SiC polytype, in particular, are expected to enable significant improvements to a far ranging variety of applications and systems [1–5]. However, since this is a relatively new technology, intensive efforts are still necessary to ascertain the detailed physics and the real design benefits that can be obtained by developing simple SiC-based devices. To this extent, in this paper different forward *J–V* behaviours of several Al implanted 4H-SiC vertical p–i–n diodes are investigated by means of measurements and numerical simulations in a wide range of currents and temperatures. In details, diode experimental data and results of a proprietary simulation software [6] are combined to extract key physical parameters, including temperature dependent carrier lifetime and mobility, which aid to differentiate the current transport mechanisms at different biases. The current–voltage characteristics of well behaved and leaky diodes, realised with the some fabrication process, are presented. In addition, the role of the diode internal resistance in determining a crossing point from a positive to a negative temperature coefficient of the current [7–9] is reconsidered by simulations.

The realization of 4H-SiC p–i–n diodes with a negative temperature coefficient of the forward current could be well suitable for stable applications using parallel devices. This study could also turn useful in the design of more complex 4H-SiC power devices, such as the various JFET-based devices recently presented in literature [10–13], where p–i–n diodes are the embedded structures determining the device on- and off-state characteristics.

2. Device structure

The schematic cross-section (plot not in scale) of the investigated Al implanted p–i–n diodes and the calculated net doping profile along the vertical axis of symmetry of a device realized using a 5 μm-thick and $3 \times 10^{15}\,cm^{-3}$-doped epilayer, are shown in Fig. 1.

The diodes were provided by the CNR Institute for Microelectronics and Microsystems – Unit of Bologna (Italy). Details about the adopted technology were provided in [7] and references therein. In short, starting from a commercially available ⟨0001⟩ 8° off-axis 4H-SiC n-type homoepitaxial wafer of elevated crystal quality [14], the diode structure consists of a n^+ substrate with a doping concentration in the order of $10^{19}\,cm^{-3}$, a $3 \times 10^{15}\,cm^{-3}$ n^- epilayer and a p^+ anode region obtained by

* Corresponding author.
E-mail address: sandro.rao@unirc.it (S. Rao).

http://dx.doi.org/10.1016/j.sse.2015.03.001
0038-1101/

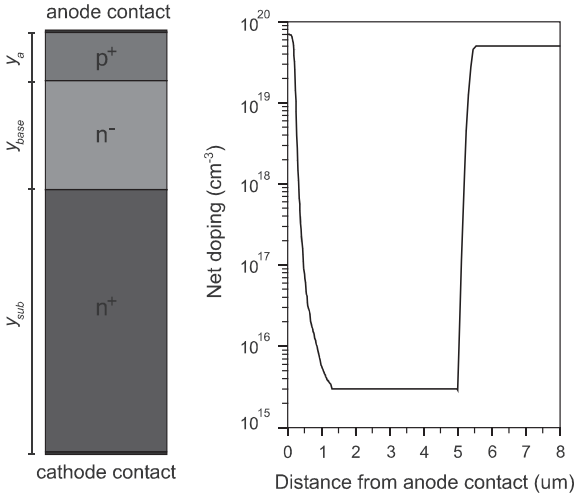

Fig. 1. 4H-SiC p–i–n diode schematic cross-section and net doping profile of a device with a 3×10^{15} cm^{-3}-doped epilayer.

aluminium implant. For the device in Fig. 1 (structure #1) the anode region exhibits a smooth half-Gaussian shaped profile with a peak doping of 6×10^{19} cm^{-3} at the surface, a profile edge located at about 0.2 μm and a profile tail crossing the epilayer doping at 1.35 μm, as verified by SIMS measurements. Almost similar diodes (structure #2) realized using a wafer with an epilayer thickness of 16.5 μm have also been analysed in this paper. The device ohmic contacts are made of a deposited Ni film on the back, while Ti/Al dots were deposited on the anode surface. Details about the implantation process and the post–implantation annealing are again reported in [7]. There, in particular, mainly depending on different post-implantation thermal treatments of the samples, two different anode contact resistances in the order of $1.25 \times 10^{-3}\,\Omega\,\text{cm}^2$ and $2 \times 10^{-5}\,\Omega\,\text{cm}^2$ were measured at room temperature for the structures labelled #1 and #2 in Table 1, respectively. For all the samples, the calculated active area is in the range $0.75–1 \times 10^{-3}$ cm^2.

3. Physical models

The simulation analysis was carried out using the Silvaco's ATLAS simulator. The fundamental 4H-SiC physical models taken into account, such as the incomplete ionization of dopants, the band-gap temperature dependence, the carrier mobility and the carrier lifetime as a function both of doping and temperature, are briefly recalled as follows.

3.1. Incomplete ionization

Due to the wide bandgap of SiC, not all doping atoms can be assumed as fully activated. Using the Fermi–Dirac statistics, the carrier concentration N_a^- and N_d^+ (i.e. the number of ionized acceptors and donors) can be calculated with the expression [15]:

$$N_{a,d}^{-,+} = N_{a,d}\left(\frac{-1+\sqrt{1+4g_{a,d}\frac{N_{a,d}}{N_{V,C}(T)}e^{\frac{\Delta E_{a,d}}{kT}}}}{2g_{a,d}\frac{N_{a,d}}{N_{V,C}(T)}e^{\frac{\Delta E_{a,d}}{kT}}}\right) \quad (1)$$

where, N_V and N_C are the hole and electron density of states varying with temperature, N_a and N_d are the p-type and n-type doping concentrations, ΔE_a and ΔE_d are the acceptor and donor energy levels, and $g_a = 4$ and $g_d = 2$ are the appropriate degeneracy factors of the valence and conduction band. Considering the nature of the doping species (i.e. Al and N), an ionization energy level $\Delta E_a = 190$ meV and $\Delta E_d = 70$ meV is assumed [16,17].

3.2. Band gap model

The temperature dependence of the 4H-SiC band-gap is [18]:

$$E_g(T) = E_{g0} - \frac{\alpha T^2}{\beta + T} \quad (2)$$

where $E_{g0} = 3.26$ eV is the assumed band-gap energy at 300 K, $\alpha = 3.3 \times 10^{-4}$ eV/K and $\beta = 0$ are specific material parameters and T is the lattice temperature.

An apparent band-gap narrowing effect as a function of the activated doping in the p-type and n-type regions, i.e. ΔE_{ga} and ΔE_{gd} respectively, is also included during the simulations according to the Lindefelt's model of the band edge displacements [19]:

$$\Delta E_{ga} = A_a\left(\frac{N_a^-}{10^{18}}\right)^{1/2} + B_a\left(\frac{N_a^-}{10^{18}}\right)^{1/3} + C_a\left(\frac{N_a^-}{10^{18}}\right)^{1/4} \quad (3a)$$

$$\Delta E_{gd} = A_d\left(\frac{N_d^+}{10^{18}}\right)^{1/2} + B_d\left(\frac{N_d^+}{10^{18}}\right)^{1/3} + C_d\left(\frac{N_d^+}{10^{18}}\right)^{1/4} \quad (3b)$$

where $A_{a,d}$, $B_{a,d}$ and $C_{a,d}$, are appropriate 4H-SiC constants.

3.3. Mobility models

The low electric field mobility is modelled by the Caughey–Thomas empirical equation validated for 4H-SiC in [20]:

$$\mu_{n,p} = \mu_{0n,p}^{\min}\left(\frac{T}{300}\right)^{\alpha_{n,p}} + \frac{\mu_{0n,p}^{\max}\left(\frac{T}{300}\right)^{\beta_{n,p}} - \mu_{0n,p}^{\min}\left(\frac{T}{300}\right)^{\alpha_{n,p}}}{1+\left(\frac{T}{300}\right)^{\gamma_{n,p}}\left(\frac{N}{N_{n,p}^{crit}}\right)^{\delta_{n,p}}} \quad (4)$$

where N is the local (total) concentration of the ionized impurities. The model parameters $\mu_0^{\min}$, $\mu_0^{\max}$, N^{crit}, α, β, δ, and γ, are taken from [18,20] and summarized in Table 2.

For high electric fields a carrier mobility reduction due to a carrier saturated drift velocity of 2×10^7 cm/s is considered as described in [10].

3.4. Carrier lifetimes

The carrier lifetimes useful to define the Shockley–Read–Hall recombination rate are modelled as functions of doping and

Table 1
Geometrical and doping parameters of different 4H-SiC p–i–n diodes.

	Structure #1 (D1)	Structure #2 (D2)
Anode thickness, Y_a (μm)	0.2	0.5
Anode doping (cm^{-3})	6×10^{19}	1×10^{20}
Base thickness, Y_{base} (μm)	4.8	16
Base doping (cm^{-3})	3×10^{15}	3×10^{15}
Cathode thickness, Y_{sub} (μm)	300	350
Cathode doping (cm^{-3})	5×10^{19}	1×10^{19}

Table 2
4H-SiC carrier mobility parameters.

	n	p
$\mu_0^{\min}$ (cm^2/V s)	40	15.9
$\mu_0^{\max}$ (cm^2/V s)	950	125
N^{crit} (cm^{-3})	2×10^{17}	1.76×10^{19}
α	−0.5	−0.5
β	−2.4	−2.15
δ	0.76	0.34
γ	−0.76	−0.34

temperature by means of a relation derived by the Scharfetter's model [10]:

$$\tau_{n,p} = \frac{\tau_{0n,p}\left(\frac{T}{300}\right)^{\lambda}}{1+\left(\frac{N}{N_{n,p}^{SRH}}\right)^{K}} \quad (5)$$

Here, N is the total doping density for a given device region, $N_{n,p}^{SRH} = 5 \times 10^{16}\ cm^{-3}$ is a reference constant, and τ_0 is a process-dependent fitting parameter.

4. Experimental results and simulations

The current–voltage measurements were realised by means of a HP4155 Semiconductor Parameter Analyser. Imposing a compliance current of 100 mA, several diodes with the structure #1 and #2 in Table 1 were characterized at different operating temperature. Almost all the samples showed good rectifying behaviours.

4.1. Room temperature analysis

The forward log(J)–V characteristics of good quality diodes labelled as D1A, D1B, D2A and D2B are shown in Fig. 2(a) and (b). For comparison, each figure also reports the characteristic of a typical "leaky" diode (D1C in Fig. 2(a) and D2C in Fig. 2(b)). The good quality diodes are characterised by a sharp turn-on at a threshold voltage close to 2 V and perform at relatively high biases a current densities in the range 10–100 A/cm^2.

By analysing with the aid of numerical and analytical simulations the electron and hole concentrations, as well as the recombination rate depth profiles of similar p–i–n structures at various voltage biases as described in [21,22], four different current regimes can be determined. In details, referring to Fig. 2(a), the current is dominated by carrier diffusion in the region (III) and recombination in the region (II). The diffusion and recombination current mechanisms produce a quick rise in slope, which is a characteristic of high quality, low resistance, and efficient operation. Conversely, the diode D1C conducts a considerably high current at the lowest voltages in region (I), which is a characteristic of conduction through tunneling phenomena. This excess current can be related to a leakage path or a shunt resistance connected in parallel with the principal (ideal) p–i–n junction. In other words, such a shunt resistance has nonlinear characteristics and then the D1C current behaviour can be modelled as due to two diodes with different barrier heights connected in parallel, each contributing to the current independently, where the defective diode has a lower turn-on voltage. This effect is most likely due to an inhomogeneous epitaxial material structure containing intrinsic defects, like micropipes, regardless of the subsequent diode fabrication process [23–25]. From the experimental analysis, a percentage in the order of 20% of the samples has been classified as "leaky" diode. Obviously, this statistic is related to the effective diode size and crystal quality of the starting 4H-SiC wafer.

Finally, at voltages higher than ~2.9 V, all diodes in Fig. 2(a) show a series resistance effect in the region (IV). Here the plots tend to become flat and the current is entirely dominated by a series resistance value that can be considered as the sum of the contact contributions and the diode internal resistance. In this region, the D1C behaviour can be related to the lack of an effective carrier injection through the junction, preventing the setup of a conductivity modulation regime in the low doped middle region.

An analogue analysis on the current transport mechanisms at different biases can be made for the samples D2 in Fig. 2(b), though they show lower current densities in region (IV) if compared to D1, as a consequence of a higher series resistance due to the thicker epilayer and lower doping of the substrate (see Table 1).

The well behaved diodes D1A and D2A were selected in order to fit with simulation results. The parts of the forward current characteristics due to recombination and diffusion phenomena are well suited as reference for the calibration of the carrier lifetime parameters. In particular, from the simulations it is evident that at low and medium current regimes, namely in the voltage bias range 1.8–2.75 V, the total diode current is strongly influenced by the effective carrier lifetime in the base region as shown in Fig. 3 for the diode D1A assuming different values of τ_0 in (5) with a ratio $\tau_{0n}/\tau_{0p} = 5$ [18].

A fitting parameter $\tau_{0n} = 10$ ns for D1A is in accordance with the experimental results measured on similar p–i–n diodes by using both the reverse recovery [26] and the open-circuit voltage decay [27] techniques. For D2A, τ_{0n} results ~3 times lower. This value is due to the existence of a higher concentration of deep-level defects produced by the Al^+ ion implantation process probably located near the metallurgical boundary of the p^+–n junction [28] and responsible of an explicit carrier recombination effect. The Al implantation into 4H-SiC epitaxial layers, in fact, yields only a fraction of Al atoms that really occupy a substitutional position in the crystal. Therefore, depending on the implantation process and the annealing conditions, a deep-centres density correlated with the non-substitutional Al concentration that produces a donor-like trap effect (the traps are positively charged when empty), with energy levels in the range 0.2–0.3 eV from the valence band edge, can be assumed [29].

4.2. High temperature analysis

Interesting diode behaviours were obtained performing a high temperature analysis for both the D1 and the D2 samples.

The measured and simulated J–V characteristics of the diode D1A at various temperatures are shown in Fig. 4 in semi-log scale.

As the temperature increases the curves tend to shift left and up. This is an explicit effect of the temperature dependence on the carrier lifetime and intrinsic carrier concentration, which are fundamental parameters in determining the recombination and diffusion components of the diode current behaviours. For example, when the testing temperature is at 378 K, the simulations indicate a carrier lifetime value that increases up to about 30 ns in the base region. At all temperatures, the simulated J–V characteristics are in good agreement with the experimental data over several decades for current.

The diode saturation current density, J_s, was also estimated from the simulations at different temperatures. The Arrhenius plot of $\ln(J_s)$ against $1000/T$ is shown in Fig. 5. The best linear fit indicates that the recombination currents determine an activation energy of 1.61 eV. This value is close to the half value of the material band-gap energy.

At the medium biases, namely between 2.5 V and 2.75 V, an ideality factor in the order of 1.3 was extracted in the considered temperature range as shown in Fig. 6.

In the series resistance region of the curves in Fig. 4 only a limited current increase is observed for voltage biases higher than 3 V. A good fit between the simulated and experimental results was achieved considering a temperature dependence of the contact resistance in the order of $-5\ \mu\Omega\ cm^2\ K^{-1}$ as experimentally measured in [7] in the 298–563 K temperature range, pointing out a mixing of thermionic and field-effect conductions through the contact-semiconductor interface. This result is also confirmed in [22] where the distributed contact resistance of similar p–i–n diodes was investigated.

In the series resistance region, however, structure #2 exhibits a different J–V–T behaviour, as shown in Fig. 7 for the diode D2A. In fact, although there are weak differences between the D1 and D2 diodes in (a) the current components related to the carrier recombination and diffusion phenomena with a positive

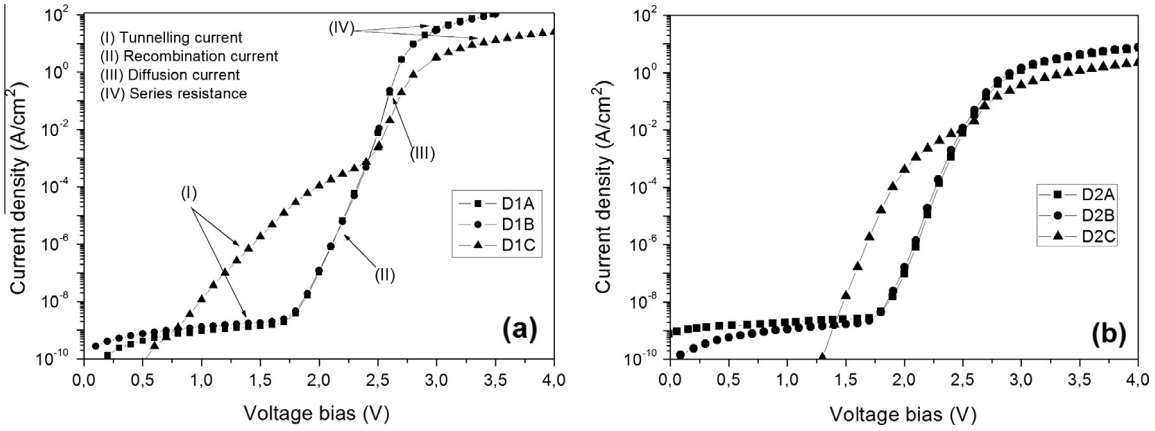

Fig. 2. Forward *J–V* characteristics of several 4H-SiC p–i–n diodes (structure #1 (a), structure #2 (b)) measured at 298 K.

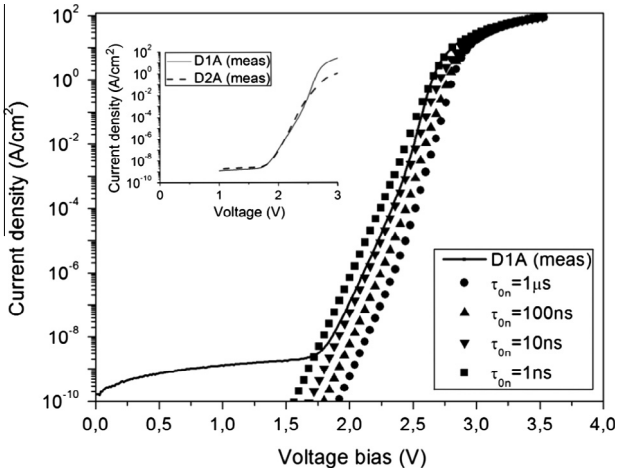

Fig. 3. Calibration of the carrier lifetime simulation parameters for the diode D1A at $T = 298$ K. The inset shows a comparison between the measured *J–V* curves of the diodes D1A and D2A.

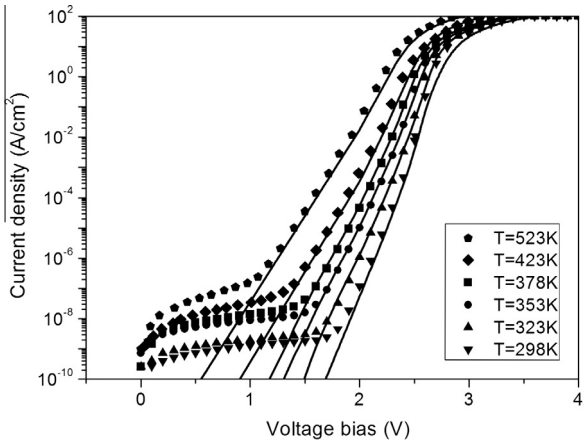

Fig. 4. Simulated (solid lines) and experimental (dot lines) forward characteristics of the diode D1A at different temperatures.

temperature coefficient, (b) the carrier lifetime increasing with temperature and (c) an ideality factor close to 2, we can note the existence for the D2 samples of a crossing point in the *J–V* characteristics as the temperature increases. In particular, for the diode D2A this point is located at a voltage bias close to 2.8 V, corresponding to a current density of 300 mA/cm^2.

Considering the diode series resistance, R_s, in the form $R_s = 2R_c + R_i$, where R_i represents the diode internal contribution and $R_c(\mathrm{D2}) < R_c(\mathrm{D1})$ as obtained from measurements [7], whereas for the diode D1A we can assume $2R_c > R_i$ (see the negative temperature coefficient of the curves in Fig. 4), in order to explain the current behaviours shown in the series resistance region of Fig. 7, it is evident that for the diode D2A the R_i effect overcomes the R_c contributions at all temperatures determining a positive temperature coefficient. In fact, since the carrier lifetime is too low to ensure a proper conductivity modulation, the diode internal contribution R_i is mainly determined by the thickness and doping of the epilayer and substrate. Therefore, the carrier mobilities decrease with temperature limits more and more the D2A current capabilities. In particular, $R_i \propto 1/qN\mu_n$ and, in fact, as a consequence of a higher dopant activated in the n^+ region that tends to suppress the hole injection in the substrate, above the *J–V* curve knee the total diode current is dominated by the electron injection into the anode. This can be explained with the incomplete ionization model, predicting a ~10 times lower saturation level of the ionized acceptor concentration with respect to donors. In other words, in the anode region the substitutional Al atoms give origin only to a limited concentration of free holes for conduction.

In order to better highlight the temperature dependence of the carrier mobility and to properly fit the measured forward characteristics of the device D2A at highest current regimes, a simplified version of (4) in the form $\mu_{n,p} = \mu_{0n,p}(T/300)^{\alpha}$ was also considered

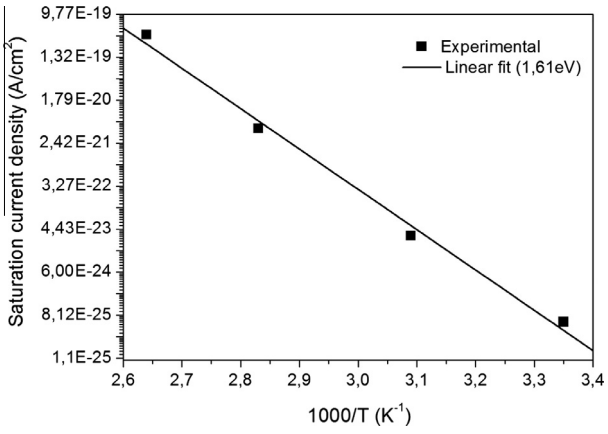

Fig. 5. Arrhenius plot of the diode D1A saturation current density.

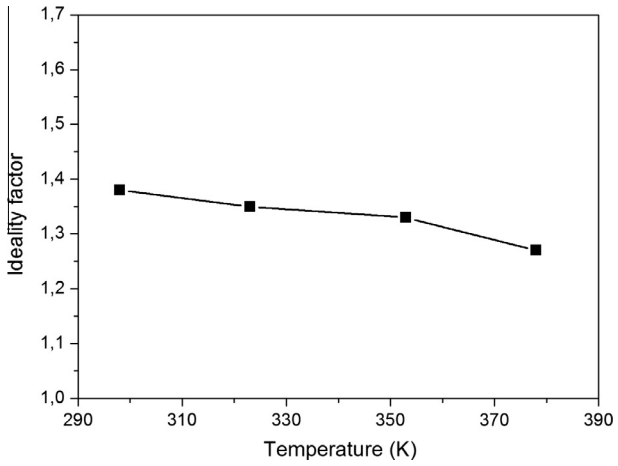

Fig. 6. Ideality factor of the diode D1A between 2.5 V and 2.75 V at different temperatures.

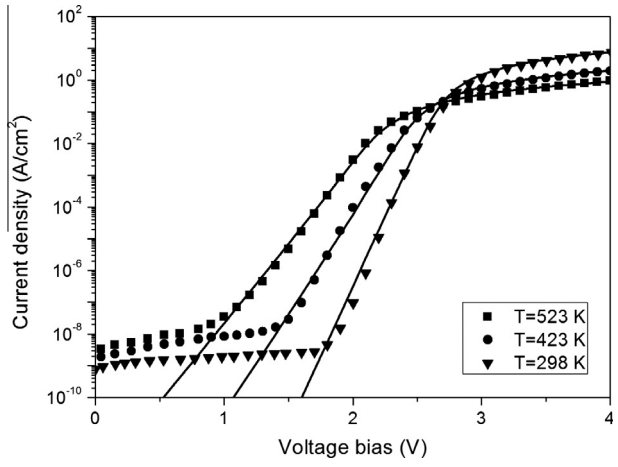

Fig. 7. Simulated (solid lines) and experimental (dotted lines) forward characteristics of the diode D2A at different temperatures.

during the simulations. Assuming $\mu_{0p} = 6\ cm^2/V\ s$ at $T = 300$ K, as measured by Hall effect in [7], the best fit gives $\mu_{0n} = 30\ cm^2/V\ s$ and $\alpha = 5.25$. Such carrier mobility should be considered a minimum value along the diode structure, predicting a diode internal resistance that can be as high as about 10 $m\Omega\ cm^2$. This result explains the limited maximum current handling of the samples D2 compared to D1.

5. Conclusion

The current–voltage characteristics of several Al implanted 4H-SiC p–i–n diodes have been presented reporting experimental and numerical results in the 298–523 K temperature range. The measured forward *J–V* curves show leaky behaved and well behaved diodes with good rectifying characteristics. The latter have been considered for simulation comparison. An excellent agreement to the measurements has been achieved by a fine tuning of the technology-dependent carrier lifetime and mobility parameters in the base region. The role of the diode resistance contributions in determining different temperature dependencies of the current behaviours has been pointed out.

Acknowledgement

The authors would like to thank R. Nipoti and the staff of the Institute for Microelectronics and Microsystems (CNR-IMM, Bologna, Italy) for supplying the 4H-SiC diodes.

References

[1] Wang R, Boroyevich D, Ning P, Wang Z, Wang F, Mattavelli P, et al. A high-temperature SiC three-phase AC–DC converter design for >100 °C ambient temperature. IEEE Trans Power Electron 2013;28(1):555–72.
[2] Lee MC, Huang AQ. An injection efficiency model to characterize the injection capability and turn-off speed for >10 kV 4H-SiC IGBTs. Solid-State Electron 2014;93:27–39.
[3] Lin L, Zhao JH. Simulation and experimental study of 3-step junction termination extension for high-voltage 4H-SiC gate turn-off thyristors. Solid-State Electron 2013;86:36–40.
[4] Moghadam H, Orouji A, Dideban A. A novel 4H–SiC SOI-MESFET with a modified breakdown voltage mechanism for improving the electrical performance. Semicond Sci Technol 2012;27:015001.
[5] Lee Wen-Shan. Design and fabrication of 4H–SiC lateral high-voltage devices on a semi-insulating substrate. IEEE Trans Electron Devices 2012;59:754–60.
[6] Silvaco Atlas User's Manual. Device Simulation Software; 17 October 2013.
[7] Nipoti R, Moscatelli F, De Nicola P. Al^+ implanted 4H-SiC p^+-i-n diodes: forward current negative temperature coefficient. Electron Dev Lett, IEEE 2013;34(8):966–8.
[8] Imhoff EA, Hobart KD, Kub FJ, Ancona MG, Myers-Ward RL, Garces NY, et al. Positive temperature coefficient SiC PiN diode. Mater Sci Forum 2012;717–720:981–4.
[9] Satoh M, Nagata S, Nakamura T, Doi H, Shibagaki M. Doping level dependence of electrical properties for p^+n 4H-SiC diode formed by Al ion implantation. Mater Sci Forum 2009;615–617:679–82.
[10] Pezzimenti F. Modeling of the steady state and switching characteristics of a normally-off 4H-SiC trench bipolar-mode FET. IEEE Trans Electron Devices 2013;60(4):1404–11.
[11] Li Y, Alexandrov P, Zhao JH. 1.88-m cm^2 1650-V Normally on 4H-SiC Ti-VJFET. IEEE Trans Electron Devices 2008;55(8):1880–6.
[12] Della Corte FG, Pezzimenti F, Bellone S, Nipoti R. Numerical simulations of a 4H-SiC BMFET power transistor with normally-off characteristics. Mater Sci Forum 2011;679:621–4.
[13] Su M, Sheng K, Li Y, Zhang Y, Wu J, Zhao J, et al. 430-V 12.4-mΩ cm^2 normally off 4H-SiC lateral JFET. Electron Dev Lett, IEEE 2006;27(10):834–6.
[14] CREE Research Inc. Durham, NC, USA <http://www.cree.com>.
[15] Ruff M, Mitlehner H, Helbig R. SiC devices physics and numerical simulation. IEEE Trans Electron Devices 1994;41:1040–54.
[16] Ayalew T, Grasser T, Kosina H, Selberherr S. Modeling of lattice site-dependent incomplete ionization in α-SiC devices. Mater Sci Forum 2005;483:845–8.
[17] Troffer T, Schadt M, Frank T, Itoh H, Pensl G, Heindl J, et al. Doping of SiC by implantation of boron and aluminium. Phys Status Solidi (a) 1997;162:277–98.
[18] Li X, Luo Y, Fursin L, Zhao JH, Pan M, Alexandrov P, et al. On the temperature coefficient of 4H-SiC BJT current gain. Solid State Electron 2003;47:233–9.
[19] Lindefelt U. Doping-induced band edge displacements and band gap narrowing in 3C-, 4H-, 6H-SiC, and Si. J Appl Phys 1998;84:2628–37.
[20] Roschke M, Schwierz F. Electron mobility models for 4H, 6H, and 3C SiC. IEEE Trans Electron Devices 2001;48:1442–7.
[21] Della Corte FG, Pezzimenti F, Nipoti R. Simulation and experimental results on the forward *J–V* characteristic of Al implanted 4H-SiC p–i–n diodes. Microelectron J 2007;38:1273–9.
[22] Bellone S, Della Corte FG, Freda Albanese L, Pezzimenti F. An analytical model of the forward *I–V* characteristics of 4H-SiC p–i–n diodes valid for a wide range of temperature and current. IEEE Trans Power Electron 2011;26:2835–43.
[23] Bolen ML, Capano MA. Defect analysis of barrier height inhomogeneity in titanium 4H-SiC Schottky barrier diodes. J Electron Mater 2009;38:574–80.
[24] Klein PB, Shanbrook BV. Lifetime-limiting defects in n-4H-SiC epilayers. Appl Phys Lett 2006;88:052110-1–0-3.
[25] Ewing DJ, Wahab Q, Ciechonski RR, Syväjärvi M, Yakimova R, Porter LM. Inhomogeneous electrical characteristics in 4H-SiC Schottky diodes. Semicond Sci Technol 2007;22:1287–91.
[26] Pezzimenti F, Della Corte FG, Nipoti R. Experimental characterization and numerical analysis of the 4H-SiC p–i–n diodes static and transient behaviour. Microelectron J 2008;39:1594–9.
[27] Bellone S, Albanese LF, Licciardo GD. A self-consistent model of the OCVD behavior of Si and 4H-SiC p+–n–n+ diodes. IEEE Trans Electron Devices 2009;56:2002–910.
[28] Levinshtein ME, Mnatsakanov T, Ivanov P, Palmour JW, Rumyantsev SL, Singh R, et al. "Paradoxes" of carrier lifetime measurements in high-voltage SiC diodes. IEEE Trans Electron Dev 2001;48:1703–10.
[29] Feng ZC, Zhao JH. Silicon carbide: materials, processing and devices. New York: Taylor & Francis; 2004 [chapters 4–5].